Chemical Geology 493 (2018) 199–209

Contents lists available at ScienceDirect

Chemical Geology

journal homepage: www.elsevier.com/locate/chemgeo

High-relief topography of the Nima basin in central Tibetan Plateau during the mid-Cenozoic time

Lihuan Deng[a,b], Guodong Jia[a,*]

[a] State key Laboratory of Marine Geology, Tongji University, Shanghai 200092, China
[b] CAS Key Laboratory of Ocean and Marginal Sea Geology, Guangzhou Institute of Geochemistry, Chinese Academy of Sciences, Guangzhou 510640, China

ARTICLE INFO

Editor: Dong Hailiang

Keywords:
Paleoelevation
Leaf wax *n*-alkane isotopes
Branched GDGT derived temperature
Multi proxies
Tibetan Plateau
Mid Cenozoic

ABSTRACT

There remains inconsistence of uplift history of the Tibetan Plateau. Here, we estimated paleoelevation of mid-Cenozoic Nima basin located in central Tibet using multi proxies. They included meteoric water and vegetation isotope proxies based on hydrogen and carbon isotopic compositions (δD and $\delta^{13}C$), respectively, of terrestrial plant wax lipid of *n*-alkanes and temperature proxy derived from microbial membrane lipid of branched glycerol dialkyl glycerol tetraethers (brGDGTs). Lipid analysis on sedimentary rocks in the Nima basin yielded −222 ± 12‰ and −30.0 ± 0.7‰ for δD and $\delta^{13}C$ of *n*-C_{29} alkane, respectively, and brGDGT-derived mean annual air temperature (MAAT) of 21.5 ± 3.1 °C for the paleo basin. Using the sea-level meteoric water $\delta^{18}O$ and Miocene Siwalik paleovegetation $\delta^{13}C$ as low elevation references, values of δD and $\delta^{13}C$ of *n*-C_{29} alkane in this study suggested paleoelevations of 4546 m and 2800 m, respectively. Whereas by using a subtropical sea surface temperature as a reference, brGDGT-derived MAATs suggested a paleoelevation of 893 m. We believed that the three estimates reflect a high-relief topography in the study basin during the mid-Cenozoic, representing elevations of orographic barrier of southerly oceanic moisture, basin catchment and basin lake level, respectively. This scenario implies a low elevation of the basin relative to the Lhasa Terrane located to the south during the mid-Cenozoic, hence challenging the classical crustal thickening models assuming a simple crustal thickening-uplift relationship.

1. Introduction

The Tibetan Plateau (TP) is the world's highest and largest orogenic plateau, with topographically low-relief surfaces. It is pieced together flat basins separated by mountain ranges tens to hundreds of kilometers apart (Liu-Zeng et al., 2008). The evolution of the plateau topography in the Cenozoic is crucial to assess the validity of models addressing plateau uplift and growth. However, the paleoelevation of the plateau is still poorly constrained in space and time albeit much effort having been made (Deng and Ding, 2015), not to mention the paleo relief that is defined as the elevation difference between the highest and lowest points in a local area.

Oxygen and hydrogen isotope compositions ($\delta^{18}O$ and δD, respectively) in materials, e.g. pedogenic carbonate and plant lipids, inherited from meteoric water are one of the most conventional methods for reconstructing paleoelevation (Poage and Chamberlain, 2001; Blisniuk and Stern, 2005; Rowley, 2007). Most paleoelevations estimated by these methods demonstrate near-modern altitudes at least during the mid-Cenozoic in the southern and central TP (e.g., Rowley and Currie, 2006; Polissar et al., 2009; Quade et al., 2011). However, an ideal relation of moisture isotope with elevation occurs only on the southern and eastern margins of the TP, and is greatly distorted in the plateau interior by factors such as different moisture sources, local surface water recycling and sub-cloud evaporation (Li and Garzione, 2017). In addition, isotope-derived high elevations disagree with results from pollen, fish and mammal fossil records arguing for lower elevations during the mid-Cenozoic in central TP (e.g., Deng et al., 2012; Sun et al., 2014; Wang and Wu, 2015).

We believe that the inconsistence of paleoelevation estimates for a specific basin likely demonstrates local significant relief due to different rationales of paleoelevation proxies, and thereby multi-proxy estimates are more robust to constrain paleo-topography than any single approach. Here, we report paleoelevation estimates for the Nima basin in central TP using multiple organic biomarker proxies, including the δD and $\delta^{13}C$ values of higher plant leaf wax *n*-alkanes and microbial tetraether-derived MBT/CBT temperature index. The ability of leaf wax δD to document the altitudinal lapse rate of meteoric water δD has been extensively verified (e.g., Jia et al., 2008b; Luo et al., 2011; Bai et al.,

* Corresponding author.
E-mail address: jiagd@tongji.edu.cn (G. Jia).

https://doi.org/10.1016/j.chemgeo.2018.05.041
Received 12 January 2018; Received in revised form 21 May 2018; Accepted 26 May 2018
Available online 28 May 2018

2012, 2015) and been applied as a paleoaltimetry (Polissar et al., 2009; Hren et al., 2010; Jia et al., 2015). The leaf wax $\delta^{13}C$ is also potential for paleoelevation reconstruction because $\delta^{13}C$ of C_3 plant shifts positively with altitude globally (Körner et al., 1988, 1991; Kelly and Woodward, 1995), and this trend has been documented in $\delta^{13}C$ values of organic matter (OM) and leaf wax *n*-alkanes in surface soils along mountain slopes (Bird et al., 1994; Wei and Jia, 2009; Wu et al., 2017). The microbial membrane lipids of branched glycerol dialkyl glycerol tetraethers (brGDGTs) are ubiquitous in soils and lake sediments (Schouten et al., 2013), and the MBT/CBT index based on the relative abundances of brGDGT compounds is powerful to reconstruct terrestrial air temperature (Weijers et al., 2007b). Since air temperature commonly decreases with increase of altitude, the MBT/CBT index has been also testified as an indicator of elevation (e.g., Sinninghe Damsté et al., 2008; Peterse et al., 2009; Liu et al., 2013; Coffinet et al., 2014; Deng et al., 2016; Wang et al., 2017; Bai et al., 2018) and recently been used to reconstruct paleoelevation (Hren et al., 2010; Decelles et al., 2018; Bai et al., 2018). In the followings, we show that the estimates of paleoelevation of the mid-Cenozoic Nima basin are different based on the above three proxies, which may reflect high-relief topography of the basin.

2. Study area, samples and analysis

2.1. Study area

The Nima basin is a Tertiary sedimentary basin situated in the central TP. It currently sits at an elevation of 4.5–5 km in the Bangong suture zone (BSZ) separating the Qiantang and Lhasa terranes to the north and south, respectively (Fig. 1B). The southern Nima basin contains > 4000 m Tertiary alluvial, fluvial, lacustrine, and lacustrine fan-delta deposits that constitute the Nima Redbed Unit (DeCelles et al., 2007a). In this study, the Dagze Co section in the Nima Redbed Unit, located between the sections 1DC and 4DC in Fig. 1 of DeCelles et al. (2007a), was sampled (Fig. 1C). According to DeCelles et al. (2007a, 2007b), the Nima Redbed Unit was deposited during the late Oligocene-early Miocene, and two tuff ages of 24.9 ± 0.1 Ma and 25.8 ± 0.2 Ma have been determined in the nearby section 1DC (Decelles et al., 2007b). A high-resolution magnetostratigraphy of the Dagze Co section has been acquired at the Paleomagnetism and Geochronology Laboratory of the Institute of Geology and Geophysics, Chinese Academy of Sciences. Based on the age controls in the nearby section 1DC, the magnetostratigraphy was correlated to the standard polarity time scale and the obtained polarity sequence was correlated to the geological time scale 2004 (GPTS OS2004), covering an age range of 28–23 Ma (Personal communication with Chunsheng Jin).

2.2. Samples and analysis

A total of 20 samples characterized by lacustrine fine-grained gray mudstone were collected in the Dagze Co section for organic geochemical measurements in this study (Fig. 1C). Samples of ~50 g were broken into 1–2 cm^3 fragments, rinsed with dichloromethane (DCM) and then pulverized to fine powders. Powdered samples were ultrasonically extracted for lipids 6 times (6×) sequentially with MeOH (2×), dichloromethane (DCM)/MeOH (1:1, v/v) (2×) and DCM (2×), and all extracts were combined after centrifugation. The solvent was removed by vacuum rotary evaporation, and then the extract was separated into an apolar fraction and a polar fraction over an activated alumina column by elution with *n*-hexane/DCM (95:5, v/v) and DCM/MeOH (1:1, v/v), respectively. The apolar fraction contained hydrocarbon compounds, an aliquot of which was used for compound

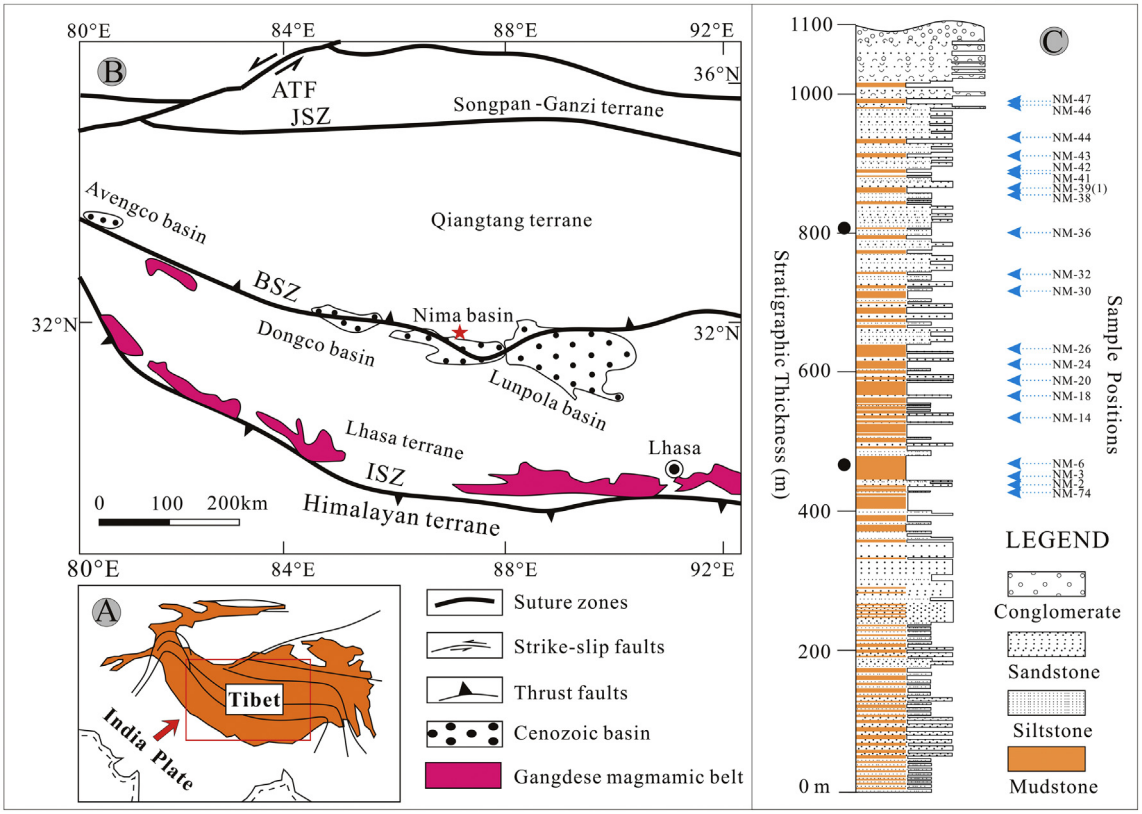

Fig. 1. A) The Tibetan Plateau. B) The geological background of the Nima basin on the Tibetan Plateau (after DeCelles et al., 2007a). ATF: Altyn Tagh fault; BSZ: Banggong suture zone; JSZ: Jingsha Suture zone; ISZ: Indus-Yarlung suture zone. C) Stratigraphic section Dagze Co from which the samples reported here were collected. Two black dots indicate the position of ages of 24.9 ± 0.1 Ma and 25.8 ± 0.2 Ma determined in the nearby section 1DC (DeCelles et al., 2007b) based on magnetostratigraphic correlation.

identification and the remaining was further purified for *n*-alkanes by urea adduction. The polar fraction contained the brGDGTs. After the solvent was removed under N_2, the polar fraction was redissolved via sonication (5 min) in hexane/propanol (99:1, v/v) and filtered through a 0.45 μm, 4 mm diameter PTFE filter before instrumental analysis.

Hydrocarbon identification for hopanes, steranes and *n*-alkanes was performed on Finnegan SSQ-7000 mass spectrometer connected with a TRACE 2000 gas chromatographer (GC–MS). The injector temperature was maintained at 290 °C. The GC oven program increased from 80 °C (held for 2 min) to 140 °C at a rate of 10 °C/min, then continued to 290 °C at 4 °C/min, and was held for 290 °C for 20 min.

The compound-specific δD and $\delta^{13}C$ values were measured using an HP 6890 gas chromatographer connected to a Finnigan DELTA plus XL isotope ratio mass spectrometer (GC-IRMS) via a high temperature thermal conversion reactor (1450 °C) and a combustion reactor (940 °C), respectively. In GC analysis module, the temperature program and capillary column were identical to those for GC–MS. The reproducibility and accuracy of δD and $\delta^{13}C$ analyses were evaluated routinely using a reference *n*-alkane mixture provided by Indiana University, with one standard injection per six sample analysis. During δD analysis the H_3^+ factor of IRMS was determined every day and its values were always < 5 ppm/nA. Besides, the peak area of each target compound was > 25 V-s, which ensures a reliable δD value on our instrument. The δD and $\delta^{13}C$ were referenced to VSMOW-water and VPDB, respectively. The standard deviations of duplicate analysis were < 6.8‰ for δD and < 0.5‰ for $\delta^{13}C$. However, some samples were analyzed only once for δD due to low abundances of *n*-alkanes.

The GDGTs were analyzed by using high performance liquid chromatograph-atmospheric pressure chemical ionization mass spectrometer (HPLC-APCI-MS) with an Agilent 1200 HPLC instrument/6410 TripleQuad MS instrument. Detection pattern was via selected ion monitoring (SIM) of $[M + H]^+$ ions (in MS1). Separation was achieved with a Prevail Cyano column (2.1 × 150 mm, 3 μm diameter particles; Grace, USA), maintained at 30 °C. GDGTs were eluted isocratically with 99% hexane and 1% propanol for 5 min, followed by a linear gradient to 1.8% propanol in 45 min. Flow rate was 0.2 ml min^{-1}. Injection volume was 10 μl. GDGTs were quantified by integration of the peak areas. The CBT and MBT indices derived from brGDGTs were calculated according to the equations established by Weijers et al. (2007b):

$$CBT = -\log([Ib + IIb]/[Ia + IIa])$$

$$MBT = [Ia + Ib + Ic]/[Ia + Ib + Ic + IIa + IIb + IIc + IIIa + IIIb + IIIc]$$

In these equations, I, II, and III represent tetra-, penta-, and hexamethylated brGDGTs, and a, b, and c represent 0, 1, and 2 cyclopentyl moieties in the alkyl backbones.

3. Results and interpretations

3.1. N-alkane distribution and thermal maturity

The carbon number of *n*-alkanes in study samples ranged from C_{16} to C_{33}. Their average abundance exhibited double peak distribution, with the former peak centered at *n*-C_{18} and the latter at *n*-C_{31} (Fig. 2A). The *n*-alkanes from C_{16} to C_{22} did not show a carbon number preference, whereas those from C_{25} to C_{33} were characterized by a prominent odd-over-even preference (OEP). These distribution features are similar to modern lake sediments that receive OM from both terrestrial plants (*n*-$C_{29–33}$, high OEP) and aquatic sources (*n*-$C_{14–20}$, low OEP). However, aquatic plants, especially submerged plants, have been recently found to also produce substantial amounts of *n*-C_{29} and *n*-C_{31} alkanes in many lakes on the TP (Aichner et al., 2010a, 2010b; Liu and Liu, 2016; W. Liu et al., 2016), which may confound the conventional use of these alkanes as an indicator of terrestrial higher plants. But in those submerged plants, mid-chain *n*-C_{23} and *n*-C_{25} are generally predominant, which was not the case in our results. Moreover, δD values of *n*-C_{29} and *n*-C_{31} in this study were clearly more negative than *n*-C_{23} and *n*-C_{25} (Fig. 2B), likely indicating different source waters for them, i.e., meteoric water for *n*-C_{29} and *n*-C_{31} and D-enriched lake water for *n*-C_{23} and *n*-C_{25} (W. Liu et al., 2016). Therefore, we believe *n*-C_{29} and *n*-C_{31} are still applicable as terrestrial plant indicators in this study.

The abundant short-chain *n*-alkanes and the long-chain OEP suggest weak post-depositional bio-degradation and/or thermal alteration; otherwise, short-chain *n*-alkanes would have been preferentially removed and the long-chain OEP diminished. Further, thermal maturity of OM was additionally evaluated using sterane and hopane isomerization indices (Peters et al., 2004). The biological R configuration in the side chain of these compounds tends to be isomerized to S configuration, leading to an equilibrium mixture of the R and S diastereomers during thermal maturation. The C_{31} homohopanes were present in all samples, and the maturity parameter of 22S/(22S + 22R) ranged between 0.34 and 0.57 (Supplementary Table S1). The C_{29} steranes were detected in 19 samples, with the maturity parameter of 20S/(20S + 20R) between 0.08 and 0.39 (Supplementary Table S1). These values indicate immature to low mature OM (Peters et al., 2004). Both indices in several samples, mostly in the lower part of the section, showed elevated values of > 0.5 and > 0.24, respectively, due likely to slightly enhanced thermal maturity (Fig. 3A).

3.2. Leaf wax δD and paleoelevation

A typical δD distribution among *n*-alkanes is shown in Fig. 2B. It showed a decrease of δD with the increase of carbon number, with *n*-C_{29}, *n*-C_{31} and *n*-C_{33} exhibiting the most negative values. Additionally, in the long-chain homologues from *n*-C_{26} to *n*-C_{33}, δD values of odd-carbon-number alkanes were markedly lower by up to 30‰ than those of the adjacent even-carbon-number ones. These patterns are common in modern and ancient samples less affected by diagenetic alteration and suggest different sources and/or biosynthetic processes for *n*-alkanes (e.g., Tuo et al., 2006; Polissar et al., 2009). δD values of long chain *n*-alkanes derived from terrestrial plants preserved in paleosols and lake sediments is one of the most promising tools for inferring changes in paleoprecipitation (e.g. Liu and Huang, 2005; Tierney et al., 2008; Rao et al., 2009). In our data, δD values of *n*-C_{27}, *n*-C_{29} and *n*-C_{31} (δD_{27}, δD_{29} and δD_{31}, respectively) were highly correlated with each other (Fig. 4; Table 1), indicating a similar hydrogen source for them. However, δD_{29} values (−222 ± 12‰) was more negative than δD_{27} (−206 ± 14‰) and more positive than δD_{31} (−231 ± 11‰). This occurrence is common for leaf wax lipids in sediments (e.g., W. Liu et al., 2016), because they are mixtures of various terrestrial plant inputs, which have different dominance of individual homologues of *n*-alkanes and exhibit substantial δD variabilities. For example, leaf wax *n*-alkanes from grasses generally contain more *n*-C_{31} and *n*-C_{33}, while from forest trees and shrubs usually have more *n*-C_{27} and *n*-C_{29} (e.g., Liu and Huang, 2005; Schäfer et al., 2016). And, grass lipids are consistently more D-depleted by 30–50‰ than trees, shrubs and forbs (Liu et al., 2006; Hou et al., 2007; Liu and Yang, 2008; Sachse et al., 2012; J. Liu et al., 2016). Therefore, changes in terrestrial vegetation driven by changes in hydroclimate may eventually affect δD values measured on individual homologues. As a result, precipitation isotope deduced from leaf wax δD in sediments may vary depending upon which homologue is used. It has been proposed that δD values of *n*-C_{29} are the most reliable and unbiased indicator for past changes in rainfall and those of *n*-C_{31} and *n*-C_{33} are likely more sensitive to grass/tree vegetation changes (Wang et al., 2013; Vogts et al., 2016). Besides, in this study, gymnosperm trees are the dominant plant type (see below) that likely produce *n*-C_{29} as the main leaf wax *n*-alkanes, hereby δD as well as $\delta^{13}C$ of *n*-C_{29} (δD_{29} and $\delta^{13}C_{29}$, respectively) is used for discussion in the following.

Because thermal alteration of OM can alter the original δD through

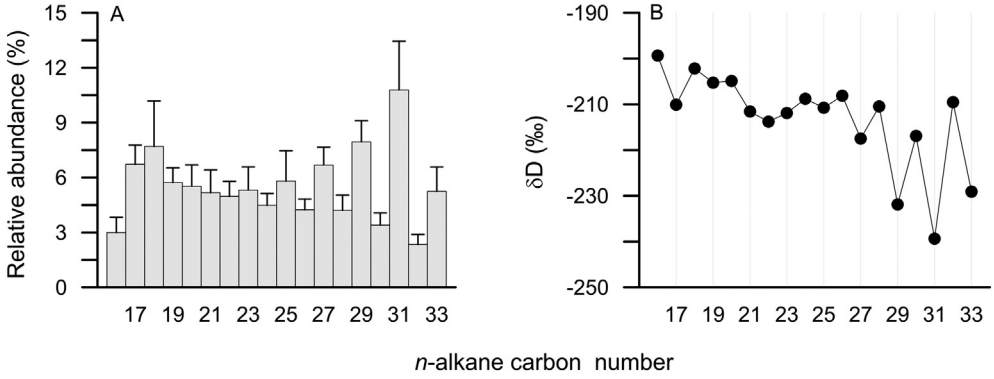

Fig. 2. (A) Average relative abundance for *n*-alkane homologues in study samples. (B) δD distribution in *n*-alkanes from a study sample (NM-39-1).

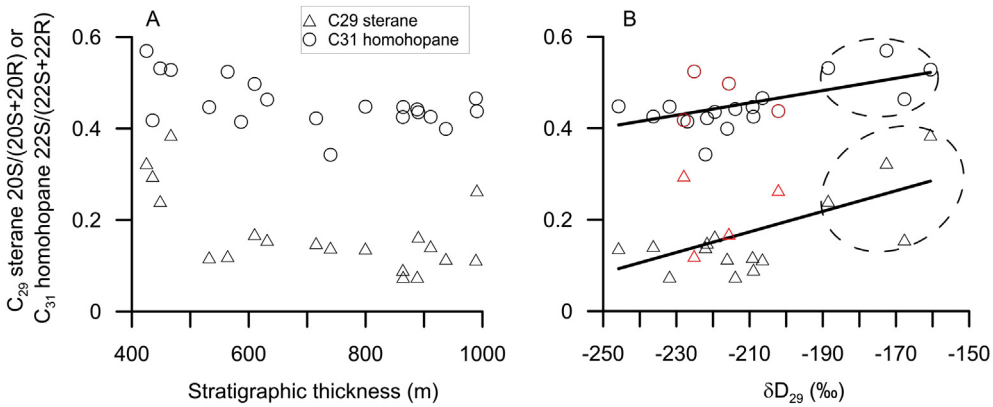

Fig. 3. The organic matter thermal maturity parameters, i.e., 20S/(20S + 20R) of C_{29} steranes and 22S/(22S + 22R) of C_{31} homohopanes, (A) in the Dagze Co section along stratigraphic thickness (thickness increases with the age decreases); and (B) their relationships with δD of *n*-C_{29} alkane. The red and rounded up symbols were excluded for subsequent paleoprecipitation and paleoelevation estimate. See details in the text. (For interpretation of the references to color in this figure legend, the reader is referred to the web version of this article.)

exchange of carbon-bound hydrogen (Radke et al., 2005; Schimmelmann et al., 2006), we also examined the impact of thermal maturity on δD_{29} as shown in Fig. 3B. There were weak positive relations of δD_{29} with the C_{29} sterane and C_{31} homohopane indices, respectively. However, the positive trends were predominantly determined by four higher values of the both indices (data points rounded up in Fig. 3B), located at the lower positions of the study section. By excluding the four samples, no trend can be seen between thermal maturity and δD_{29}, indicating little diagenetic and thermal impact on δD_{29} for the remaining samples. Nevertheless, four additional samples were further excluded for robust application of δD_{29} as source water proxy. These four samples exhibited relatively higher maturity values, with two showing C_{31} homohopane index of 0.50 and 0.52 and the other two showing C_{29} sterane index values of 0.27 and 0.30 (Supplementary Table S1).

The diagenetically and thermally unaltered δD_{29} in study samples based on above examination showed a mean value of −222 ± 12‰ (n = 12; Table 1). In recent years, there have been several works reporting leaf wax δD in surface soils and lake sediments on the TP, which allows a comparison between the past and the present. Considering that the paleolatitude of the Nima basin was similar to present (e.g., Chen et al., 2017; Meng et al., 2017), such a comparison was confined to the southern TP (< 30°N; > 4000 m altitude) in order to minimize present continental effect on moisture isotopes (e.g., Bai et al., 2012; Li and Garzione, 2017). We found our δD_{29} values were quite similar with reported values. For example, δD_{29} ranges from −240‰ to −193‰ with a mean of −222 ± 18‰ in surface sediments of five lakes (Mügler et al., 2008; Aichner et al., 2010b; Bird et al., 2014) and from −264‰ to −211‰ with a mean of −231 ± 14‰ in surface soils (n = 33; Bai et al., 2012, 2015; Wang et al., 2017). In TP south of ~30°N, δD_{29} in soils increases with the decrease of altitude (Bai et al., 2012, 2015). Thereby, the similarity of our δD_{29} values with those

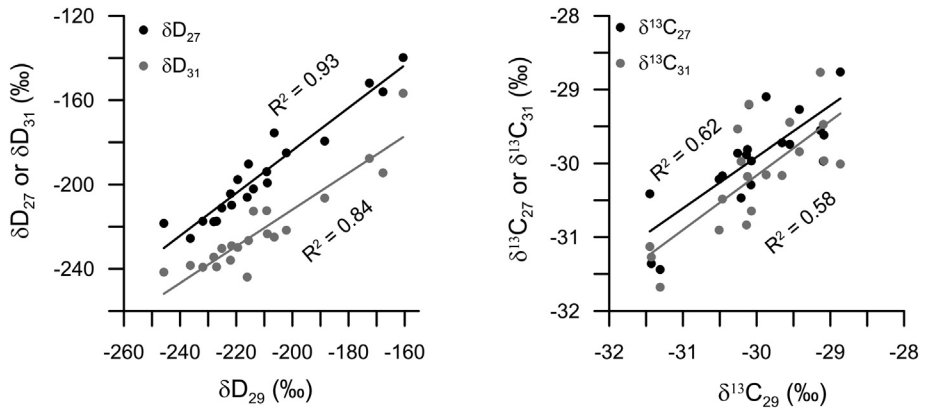

Fig. 4. Relationship of isotope compositions of *n*-C_{29} with *n*-C_{27} and *n*-C_{31} alkanes, respectively, in study samples in the Nima Basin.

Table 1
The δD and $\delta^{13}C$ values (‰, relative to VSMOW-water and VPDB, respectively) of leaf waxes *n*-alkanes, and brGDGT-derived CBT and MBT.

Sample ID	Depth	δD_{27}	δD_{29}	δD_{31}	$\delta^{13}C_{27}$	$\delta^{13}C_{29}$	$\delta^{13}C_{31}$	CBT	MBT
NM-47	990.4	−185	-202[a]	−222	−30.0	−29.1	−29.5	–	–
NM-46	988.7	−176	−206	−225	−29.6	−29.1	−28.8	–	–
NM-44	937.4	−206	−216	−244	−30.3	−30.1	–	0.31	0.46
NM-43	911.3	−226	−236	−238	−30.2	−30.5	−30.9	0.21[b]	0.36[b]
NM-42	890.2	−198	−220	−230	−29.7	−29.7	−30.2	0.28[b]	0.36[b]
NM-41	888.5	−202	−214	−213	−30.4	−31.5	−31.1	0.44[b]	0.38[b]
NM-39-1	864.3	−217	−232	−239	−31.4	−31.3	−31.7	0.20[b]	0.41[b]
NM-38	863.7	−199	−209	−223	−30.5	−30.2	−30.0	0.18	0.43
NM-36	799.6	−218	−246	−242	−30.0	−30.1	−30.6	0.14	0.53
NM-32	739.9	−204	−222	−236	−29.1	−29.9	−30.2	–	–
NM-30	715.4	−210	−222	−229	−29.3	−29.4	−29.8	–	–
NM-26	631.6	−156	−168 [a]	−195	−29.7	−29.6	−29.4	0.50	0.58
NM-24	610.1	−190	−216[a]	−227	−29.8	−30.1	−30.2	0.23	0.40
NM-20	586.8	−217	−227	−239	−29.9	−30.1	−30.8	–	–
NM-18	563.9	−211	−225[a]	−230	−31.4	−31.4	−31.3	0.37	0.49
NM-14	532.4	−194	−209	−212	−30.2	−30.5	−30.5	0.25	0.36
NM-06	466.7	−140	−161[a]	−157	−29.2	−30.1	−29.2	0.34	0.36
NM-03	448.4	−180	−189[a]	−207	−29.6	−29.1	−30.0	−0.37	0.23
NM-02	435.4	−218	−228[a]	−235	−28.8	−28.9	−30.0	–	–
NM-74	425.0	−152	−173[a]	−188	−29.9	−30.3	−29.5	0.44	0.59

– not detected.
[a] Values were not used for calculating meteoric δD as discussed in the text.
[b] Values were not used for calculating temperature as discussed in the text.

modern data could imply a high altitude (> 4000 m) of the south TP during the mid-Cenozoic, as calculated below in detail.

We used δD_{29} values to estimate paleo meteoric water δD (δD_p). The apparent fractionation between the two, i.e., $\varepsilon_{C29/p} = [(\delta D_{29} + 1000) / (\delta D_p + 1000)] - 1$, has been found varying in a large amplitude, which is associated with local geographical/climatic conditions and vegetation types (e.g., Sachse et al., 2012; Bai et al., 2015). For $\varepsilon_{C29/p}$ estimation, influences of local geographical and/or climatic conditions in the past are hard to constrain, but that of vegetation could be semi-quantified by pollen analysis and comparison with modern data (Hou et al., 2008; Sachse et al., 2012; J. Liu et al., 2016). Pollen analysis from 7 of our samples showed that gymnosperm was predominant (58.3%–97.1% range, 86.3% average), with minor angiosperm (1.4%–36.6% range, 8.7% average) and ferns (1.1%–11.6% range, 4.9% average) (Personal communication with Fuli Wu). According to the compilation of modern data by Sachse et al. (2012), gymnosperm, C_3 dicots (here we surmise angiosperm were mainly C_3 dicots because C_4 grasses expanded later in the late Miocene (e.g., Tipple and Pagani, 2007)) and ferns are similar in $\varepsilon_{C29/p}$ values, i.e., −110 ± 24‰, −113 ± 30‰, −108 ± 7‰, respectively. Recently, a more comprehensive data show similar $\varepsilon_{C29/p}$ values for gymnosperm (−106‰) and dicots (−107‰) (J. Liu et al., 2016). So, we simply applied −110 ± 24‰ for gymnosperm as the $\varepsilon_{C29/p}$ value for our samples. By using this value, the δD_{29} were then converted to δD_p, yielding a mean δD_p value of −125 ± 13‰, ranging from −153‰ to −108‰ (Supplementary Table S1). Here, we adopted the premise that sites located on the southern TP received southerly moisture dominantly from the Indian Ocean, regardless of plateau development (DeCelles et al., 2007b; Polissar et al., 2009; Quade et al., 2011). Then δD_p was recasted as $\delta^{18}O_p$ according to the global meteoric water line (GMWL), i.e., $\delta D = 8 \times \delta^{18}O + 10$, yielding a mean $\delta^{18}O_p$ value of −16.9 ± 2.0‰, ranging between −20.3‰ and −14.8‰. This mean value is close to the $\delta^{18}O_p$ value of −14.3‰ that has been calculated from corrected soil carbonate $\delta^{18}O$ (i.e., −14.4‰) by assuming a carbonate forming temperature of 14 °C (DeCelles et al., 2007b). Further, actual $\delta^{18}O_p$ may have been lower than the value derived from soil carbonate owing to possible evaporation in paleosol water (DeCelles et al., 2007b), hence likely more close to the δD_{29}-derived value here. Therefore, compared with soil $\delta^{18}O$, plant-wax δD values likely provide an estimate for precipitation δD that is less changed by evaporation. Similar conclusion has been drawn by several authors (e.g., Mügler et al., 2008; Polissar et al., 2009).

In this study, paleoelevations were calculated using two different methods: one was according to the isotope-elevation model based on the Rayleigh distillation with a temperature-dependent isotopic fractionation factor (Rowley et al., 2001; Rowley and Currie, 2006; Rowley, 2007), the other was the application of the altitudinal lapse rate of δD_p. Both methods used a low-elevation reference, which is the sea-level moisture at the tropical ocean as has been applied by others (e.g., Quade et al., 2011; Gébelin et al., 2013). The $\delta^{18}O$ value for sea-level moisture in tropical source region has been estimated to be −5.8‰ during the latest Oligocene–early Miocene (Quade et al., 2011; Gébelin et al., 2013), and the corresponding δD value is −36‰ based on GMWL. Thereby, the mean offsets in precipitation isotope composition ($\Delta\delta^{18}O_p$ and $\Delta\delta D_p$, respectively) between the Nima basin and the seal level were ca. −11.1‰ (from −14.5‰ to −9.0‰) for $\Delta\delta^{18}O_p$ and −89‰ (−117‰ to −72‰) for $\Delta\delta D_p$. By using the quartic equation presented in Rowley (2007), the $\Delta\delta^{18}O_p$ values yielded a mean elevation of 4546 ± 340 m (n = 12), with +1σ model uncertainties in the range of 717 to 997 m and −1σ model uncertainties of −1189 to −889 m (Supplementary Table S1). As to the lapse rate of δD_p, global values in the range of −10‰ to −40‰/km have been reported in literature (Ramesh and Sarin, 1992; Araguas-Araguas et al., 2000; Mulch et al., 2006), and in the southeast TP they vary in a narrower range from −14‰ to −24‰/km (Bai et al., 2015 and references therein). By using a mean δD_p lapse rate of −19‰/km here, $\Delta\delta D_p$ values resulted in a mean altitude of 4680 m (from 3800 to 6160 m), quite similar to the results from the Rowley's model.

The agreement between the above two methods indicates that (1) our conversion of leaf wax-derived δD_p to $\delta^{18}O_p$ according to GMWL for the Nima basin is feasible because the leaf wax-derived δD_p was not converted to $\delta^{18}O_p$ in the method using the δD_p lapse rate, and (2) the rainout process during moisture transport to the paleo Nima basin is consistent with Rayleigh distillation.

3.3. Leaf wax $\delta^{13}C$ and paleoelevation

The $\delta^{13}C$ of the long-chain odd-carbon-numbered *n*-C_{27}, *n*-C_{29} and *n*-C_{31} were similar in mean values (−29.9 ± 0.6‰ for $\delta^{13}C_{27}$; −30 ± 0.7‰ for $\delta^{13}C_{29}$; −30.2 ± 0.6‰ for $\delta^{13}C_{31}$) and positively

correlated with each other (Fig. 4, Table 1). Values of $\delta^{13}C_{29}$ in the 20 samples were between −31.5‰ and −28.9‰, with an average of −30.0 ± 0.7‰. According to Tipple et al. (2010), $\delta^{13}C$ of atmospheric CO_2 during the latest Oligocene and early Miocene are ca. −6.0‰, thus yielding a value of −24.0 ± 0.7‰ for the apparent carbon isotopic discrimination for *n*-C_{29} ($\varepsilon_{C29\text{-}CO2}$) in our data. This $\varepsilon_{C29\text{-}CO2}$ value is well within the range, but slightly higher than the average of −26.5‰, for C_3 plants between −33‰ and −19‰ compiled by Jia et al. (2012). In this study, the contribution of C_4 plants was not considered, because it has been well established that C_4 grasses are not a significant component in tropical ecosystem until the late Miocene (e.g., Tipple and Pagani, 2007).

It has been found that carbon isotope discrimination during photosynthesis of terrestrial C_3 plants in global wet areas decreases with altitude irrespective of plant life form and taxonomic group (Körner et al., 1988, 1991). This occurrence could be associated with greater carboxylation efficiency at high altitudes due mainly to changing partial pressures of CO_2 and/or O_2 under systematic changes of temperature, precipitation and vegetation with elevation (Körner et al., 1991; Kelly and Woodward, 1995). Although the range of reported C_3 species-level response to elevation is large (e.g., −0.9% to +2.7% km^{-1}; Körner et al., 1991), the average response to elevation based on thousands of C_3 plant species is +1.2 ± 0.9‰/km varying between +1.1‰/km and +1.3‰/km from numerous mountain ranges of the globe (e.g., Körner et al., 1988, 1991; Li et al., 2007). A more recent study on $\delta^{13}C$ of bulk plant leaves and leaf wax *n*-alkanes across an elevation gradient on the eastern flank of the Andes Mountains also reveals robust trends of +0.87 ± 0.16‰/km and +1.45 ± 0.33‰/km, respectively (Wu et al., 2017). Although drought condition has been argued to confound this trend (e.g., Van de Water et al., 2002), numerous studies still show that C_3 plants increase in $\delta^{13}C$ with altitude on the arid TP (annual mean precipitation < 500 mm) (e.g., Qiang et al., 2003; Wang et al., 2003; Li et al., 2006; Liu et al., 2007; Wang et al., 2008). Typical vegetation on present TP above 4000 m are alpine meadow and steppe, the $\delta^{13}C$ of which has been reported with a mean value of −25.5 ± 1.7‰ (n = 79; Xu et al., 2010) or −25.4 ± 0.9‰ (n = 88; Yang et al., 2015) in large-scale investigations. Recently, C_4 grasses are discovered in the warmest months on the Tibetan Plateau, but they account for negligible amounts of the biomass (e.g., Wang et al., 2008). Comparatively, $\delta^{13}C$ of C_3 plants in low altitudes are evidently lighter, e.g., −29.5‰ in Nepal south of TP (250–800 m altitude; Pokharel et al., 2015) and −29.6‰ on the foot of Mount Gongga east of TP (~1000 m altitude; Li et al., 2009). According to the average $\delta^{13}C$ altitudinal increase of 1.2‰/km, the modern $\delta^{13}C$ difference of ca. 4‰ between the high and low altitudes corresponds to ca. 3300 m elevation difference, which is roughly consistent with the fact.

However, due to the high variability of this trend among plant species, it is necessary to know whether the overall vegetation trend can be documented in sedimentary archives before its utilization for paleoelevation reconstruction. Indeed, it has been shown that soil $\delta^{13}C_{org}$ can provide useful estimators of vegetation isotopic composition, and when compared to the measurements of the vegetation, it offers the advantage of an easily obtained value that naturally integrates over plant material and time (e.g., Balesdent et al., 1993; Powers and Schlesinger, 2002; Yang et al., 2015). Such integration may benefit palaeo-ecological or biogeochemical studies at higher spatial scales (e.g. landscape or region) (Männel et al., 2007). In fact, the average species-level $\delta^{13}C$ response of C_3 plants to elevation has been found to be well recorded in the underlying soil organic carbon (Bird et al., 1994; Powers and Schlesinger, 2002; Lü et al., 2004; Wei and Jia, 2009), suggesting that the average responsive trend on species level may be scaled up linearly to community and landscape levels. Moreover, soil data show less scatter than the vegetation, indicating that soil $\delta^{13}C_{org}$, as an integrator, may reduce some of the species- and tissue-specific variability in $\delta^{13}C$ (Bird et al., 1994; Wei and Jia, 2009). More recently, this occurrence has been found true even in the semi-arid to arid Qilian Mountain area, NE Tibetan Plateau (Zhao et al., 2017). However, soil OM is subject to degradation and admixture of microbial biomass, which would alter its isotopic composition, thereby discounting its reliability as paleo-ecological indicators (Ehleringer et al., 2000). Comparatively, leaf wax *n*-alkanes are specific for higher plants, resistant to degradation and ubiquitous in sediments, allowing it to be a widely used proxy of land vegetation (Eglinton and Eglinton, 2008). An investigation on $\delta^{13}C$ of OM and leaf wax *n*-alkanes preserved in surface soils along the east slope of Mount Gongga reveals paralleled altitudinal trend between the two, showing increase of $\delta^{13}C$ with elevation (1.2‰/km) above ~2000 m, where C_4 plants are likely absent (Wei and Jia, 2009). Vegetation $\delta^{13}C$ on the same slope, albeit showing great variability among species, confirm such a trend (1.3‰/km) (Li et al., 2009). Therefore, leaf wax $\delta^{13}C$ in sedimentary archives is a potential proxy for paleoelevation.

In the low-elevation Siwalik foreland south of Himalayas (likely < 500 m; e.g. Polissar et al., 2009), $\delta^{13}C_{29}$ has been estimated to be −33.4 ± 1.5‰ during the latest Oligocene–early Miocene (Jia et al., 2015). So, the offset of $\delta^{13}C_{29}$ between the Nima basin and Siwalik foreland is 3.4 ± 1.6‰, which could have combined the influences of altitudinal and local climatic differences. Not considering the climatic influence, a mean paleoelevation difference can be calculated to be 2800 ± 629 m (n = 20; Supplementary Table S1) by applying an elevational $\delta^{13}C$ gradient of 1.2‰/km for terrestrial ecosystem (Körner et al., 1988; Wei and Jia, 2009). An uncertainty of this method was estimated to be 1330 m that is mainly derived from the uncertainty of $\delta^{13}C_{29}$, i.e., ± 1.5‰, in the low-elevation Siwalik.

Comparatively, the $\delta^{13}C$ values of modern and late Oligocene soil carbonate in the Nima area, reflective of mixing of atmospheric CO_2 with plant-derived CO_2, are −0.3‰ and −2.9‰, respectively (DeCelles et al., 2007b). Such a difference could suggest higher soil respiration rates, and hence a wetter late Oligocene climate than modern in the Nima area, although an aridity climate was proposed by DeCelles et al. (2007b). Alternatively, however, the carbonate isotope difference may likely be caused by a lower elevation, i.e., ~2000 m lower, during the late Oligocene, consistent with our lipid $\delta^{13}C$ estimate.

3.4. MBT/CBT temperature and paleoelevation

The brGDGTs were detected in 14 out of 20 samples (Supplementary Table S1). Averagely, the fractional abundance of brGDGT-Ia was similar to brGDGT-IIa and generally two times more than brGDGT-IIIa (Fig. 5B). The relative amount of cyclopentane ring-containing brGDGTs was generally lower and sometimes not detectable except for two samples. The CBT values were 0.25 ± 0.21, with most in the range of 0.18–0.50 except one extreme of −0.37. The MBT ranged between 0.23 and 0.59 and averaged 0.42 ± 0.10 (Table 1).

BrGDGTs are produced by heterotrophic acidobacteria (e.g., Sinninghe Damsté et al., 2011). Weijers et al. (2007b) first demonstrate that variations in the distributions of the nine brGDGTs are correlated to environmental conditions in globally distributed soils and develop calibrations to mean annual air temperature (MAAT) and soil pH based on MBT and CBT. This soil-based calibration has been used to reconstruct MAAT in marine sediments (Weijers et al., 2007a), loess (Peterse et al., 2011; Jia et al., 2013), and lake sediments (Fawcett et al., 2011). However, its application to lakes generally appears to be complicated by in situ production of brGDGTs in the water column and/or sediment (Sinninghe Damsté et al., 2009; Tierney and Russell, 2009; Tierney et al., 2012). Recently, several lake-specific calibrations incorporating the potential aquatic contribution of brGDGTs have been developed, thereby enabling reconstruction of palaeotemperature based on brGDGT distributions in lake sediments (Tierney et al., 2010a, 2010b; Pearson et al., 2011; Sun et al., 2011; Loomis et al., 2012), although the controls on aquatic brGDGT production remain far from being understood. The aquatic origin of brGDGTs can be distinguished

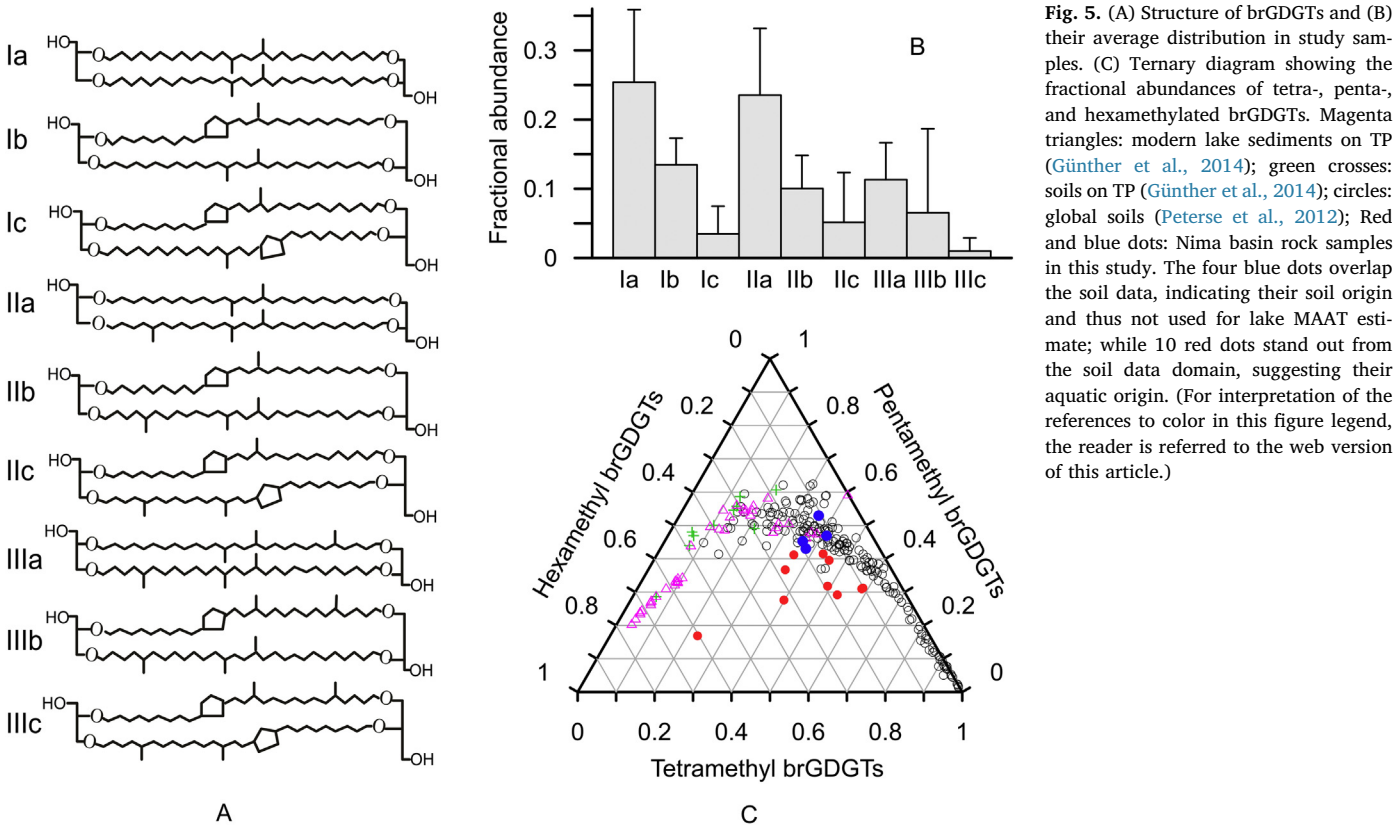

Fig. 5. (A) Structure of brGDGTs and (B) their average distribution in study samples. (C) Ternary diagram showing the fractional abundances of tetra-, penta-, and hexamethylated brGDGTs. Magenta triangles: modern lake sediments on TP (Günther et al., 2014); green crosses: soils on TP (Günther et al., 2014); circles: global soils (Peterse et al., 2012); Red and blue dots: Nima basin rock samples in this study. The four blue dots overlap the soil data, indicating their soil origin and thus not used for lake MAAT estimate; while 10 red dots stand out from the soil data domain, suggesting their aquatic origin. (For interpretation of the references to color in this figure legend, the reader is referred to the web version of this article.)

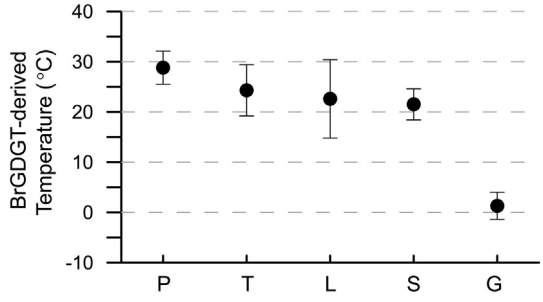

Fig. 6. Br-GDGTs-derived temperatures applying different lake calibrations to this study.
P: $T = 2.9 + 98.1 \times f_{Ib} - 12.0 \times f_{IIa} - 20.5 \times f_{IIIa}$ (Pearson et al., 2011).
T: $T = 50.47 - 74.18 \times f_{IIIa} - 31.6 \times f_{IIa} - 34.69 \times f_{Ia}$ (Tierney et al., 2010a, 2010b).
L: $T = 22.77 - 33.58 \times f_{IIIa} - 12.88 \times f_{IIa} - 418.5 \times f_{IIc} + 86.4 \times f_{Ib}$ (Loomis et al., 2012).
S: $T = 6.803 - 7.06 \times CBT + 37.09 \times MBT$ (Sun et al., 2011).
G: $T = -3.84 + 9.84 \times CBT + 5.92 \times MBT'$ (Günther et al., 2014).

by comparison of brGDGT distribution between sediments and soils. Here, we used a ternary diagram showing the fractional abundances of tetra-, penta-, and hexamethylated brGDGTs (Fig. 5C). In the diagram, 10 out of 14 of our data stand out from the global soil domain (Red dots in Fig. 5C). Similar occurrence for data outside the soil trend in the ternary diagram has been proposed to indicate in situ brGDGT production in marine environments (Sinninghe Damsté, 2016). Therefore, these 10 sample data could be suitable for paleotemperature reconstruction by using lake calibrations. By applying different calibrations to these data, our brGDGTs yielded temperature values showing discrepancies from 1.3 to 28.8 °C (Fig. 6). Temperature discrepancy between different brGDGT calibrations is common in literature, due likely to the influences of other variables such as pH, salinity, microbial production seasonality, etc. (e.g., Pearson et al., 2011; Sun et al., 2011; Günther et al., 2014). The local lake calibration from the TP by Günther et al. (2014), which produced lowest temperature of 1.3 ± 2.7 °C (Fig. 6), should have been appropriate for this study. However, the MAATs from which this calibration has been made range from −2 to +4 °C, likely only appropriate for, e.g., the late Quaternary TP that has similar elevation and environments to present. Moreover, brGDGT distributions in this study were also distinct from those in modern lakes and soils on the TP (Fig. 5C), suggestive of different biological source of brGDGTs in the paleo Nima lake from modern Tibetan lakes and hence against the use of the modern local lake calibration. Applications of other lake calibrations by Pearson et al. (2011), Tierney et al. (2010a, 2010b), Loomis et al. (2012) and Sun et al. (2011), respectively, yielded mean values of 28.8 ± 3.3 °C, 24.3 ± 5.1 °C, 22.6 ± 7.8 °C and 21.5 ± 3.1 °C (Fig. 6). Here we prefer to accept the global MAAT calibration by Sun et al. (2011), because it contains various lakes covering wide ranges of climatic conditions, lake sizes and depths. Moreover, these lakes are located at various altitudes from close to sea level to as high as 4.4 km on the southern TP. In addition, this calibration produced a narrowest temperature range (SD = ± 3.1 °C, $n = 10$) among the four calibrations. The calibration derived by Pearson et al. (2011), using the fractional abundances of brGDGT-Ib, -IIa and -IIIa, generated highest temperatures among the four calibrations, but may be compatible with the MAAT values from the calibration of Sun et al. (2011), because Pearson et al. (2011) specifically use summer air temperatures for their calibration, suggesting that these higher estimates should reflect summer temperatures.

Temperature lapse rate is a prominent feature for elevation gradient, making it a promising proxy for paleoelevation reconstruction (Stone and Carlson, 1979; Mokhov and Akperov, 2006; Kattel et al., 2013). Taking the nearby weather station of Bange (31.4°N, 90°E, 4.7 km altitude) as an example, the MAAT is −1.3 °C during the period 1957–1979 (data from www.cma.gov.cn). Comparatively, based on a global sea surface temperature (SST) climatology, SST at 30°N during 1950–1979 is 22 °C (Shea et al., 1992). Thereby, not accounting the

temperature difference between water and air at the sea level, a temperature lapse rate of ~5.0 °C/km can be estimated. This lapse rate is well within modern terrestrial temperature lapse rate (TTLR) of 4.6–6.6 °C/km between 20 and 30° N around the central-east Himalayas, i.e. in the south, north and east of Himalayas, covering a wide range of climatic and topographic conditions (Li et al., 2005; Wangda and Ohsawa, 2006; Kattel et al., 2013; Guo et al., 2015). The paleolatitude of the Nima basin was likely similar to the present, i.e. ~30° N, during the late Oligocene (e.g., Chen et al., 2017; Meng et al., 2017), when the SST at the latitude has been not well constrained. But it appears that tropical SST is similar to or slightly higher than the present (Stewart et al., 2004; Zhang et al., 2013; Tremblin et al., 2016) during the Oligocene after the growth of the first permanent Antarctic ice sheets at the Eocene − Oligocene Transition at ~33.7 Ma. The tropical SST is also similar to present during the Pliocene (Brierley and Fedorov, 2010), suggesting little changes of SST in the tropics since the Oligocene. The Neogene global cooing manifests mainly in higher latitudes, leading to a marked increase of meridional SST gradient at the late Pliocene-early Pleistocene associated with the onset of Northern Hemisphere Glaciation (NHG) (Jia et al., 2008a; Brierley and Fedorov, 2010). Before the onset of NHG, an SST value of 26.5 °C at 30°N can be estimated from the well-constrained meridional SST gradient in the northern Hemisphere during the early Pliocene (Brierley and Fedorov, 2010). Here, we surmised that the meridional SST gradient during the late Oligocene is similar to the early Pliocene, and accordingly the SST of 26.5 °C was used to constrain the paleoelevation of the Nima basin. In this way, the average temperature difference between sea level and the paleo Nima basin during the late Oligocene was 5.0 ± 3.1 °C (1.0 °C to 8.9 °C range, $n = 10$). We also surmised that the modern regional TTLR of 4.6–6.6 °C/km, i.e. 5.6 ± 1.0 °C/km, is also applicable to the mid-Cenozoic. By using this TTLR value, the temperature differences between sea level and the Nima Basin gave a paleoelevation of 893 ± 549 m ($n = 10$) (Supplementary Table S1). A method uncertainty was estimated to be 954 m that was mainly derived from the uncertainty of paleo MAAT estimates in the Nima basin (± 5.24 °C according to Sun et al., 2011).

4. Discussions and implications

There are significant differences in paleoelevation estimates of inland basins by using different methods in literature. Taking the Nima basin as an example, DeCelles et al. (2007b) propose a high paleoelevation of 4.5–5 km, comparable to today's scenario, by 26 Ma using the data of paleosol carbonate $\delta^{18}O$; whereas Wang and Wu (2015) suggest a tropical-subtropical lowland based on a new genus and species of cyprinid fish found in the same strata. In the nearby contemporaneous Lunpola basin located also in the BSZ, high elevation > 4 km is also proposed by using the paleosol carbonate $\delta^{18}O$ and leaf wax δD methods (Rowley and Currie, 2006; Polissar et al., 2009); however, a lower elevation of ca. 3 km has been argued for according to pollen, mammal fossil and leaf wax isotope records (Deng et al., 2012; Sun et al., 2014; Jia et al., 2015).

In this study, three different elevations were yielded for the same basin. We believe that the inconsistence should be attributed to different rationales of the paleoelevation proxies, as sketched in Fig. 7. For the paleo Nima basin, it should have located at leeward side of an orographic barrier, likely the Lhasa Terrain to the south, for the southerly Indian Ocean moistures (DeCelles et al., 2007a, 2007b), although a specific moisture path cannot be determined in this study. This condition might be similar to the rain shadow of the modern Sierra Nevada of California and Washington Cascades, where the stable isotopic compositions of meteorically derived surface waters are distinctly lower in comparison to those in the western windward sides, indicating a rain-shadow effect (Poage and Chamberlain, 2002; Takeuchi and Larson, 2005). Moreover, continued Rayleigh distillation of air masses in the leeward side may lead to increasing ^{18}O- and D-depletion even at lower altitudes (i.e., inverse isotope-altitude gradients; Moran et al., 2007), indicating that δD_p in the lee reflects not local elevation as described in the model of Rowley et al. (2001) but largely the elevation of the moisture barrier (Fig. 7). In this study, therefore, regardless of other confounding factors, we consider that moisture and precipitation isotopes in the Nima basin, as well as in the BSZ, may indicate altitude of the southern Lhasa Terrain barring the Indian oceanic moistures, not the local elevation of the basin. This scenario could also be applicable to the $\delta^{18}O$-based paleoelevation reconstruction using pedogenic or lacustrine carbonate on the southern TP. In comparison, $\delta^{13}C$ of terrestrial vegetation may have documented local conditions, such as climate and partial pressure of CO_2 and O_2, and hence, $\delta^{13}C_{29}$ in lake sediments may reflect the hypsometric mean elevation of the drainage basin that is generally skewed towards the lower elevations of a watershed (Fig. 7). In other word, this mean elevation is most likely biased towards the locality that contributed highest terrestrial OM input to the final lacustrine deposition site, thereby should be significantly lower than the southern moisture barriers indicated by the δD_{29} in this study. Finally, brGDGTs in lake sediments could have mixed origins from both allochthonous production in soils and autochthonous production in the lake (e.g., De Jonge et al., 2014; Sun et al., 2011; Peterse et al., 2014), which might complicate the derived temperature interpretation. However, as shown previously, our data indicate that brGDGTs in 10 samples of the Nima basin were dominantly aquatic origin, allowing us to choose a lake calibration for temperature reconstruction. In practice, the CBT/MBT temperature proxy is calibrated to MAATs at the lake sites (Sun et al., 2011), thereby may reflect MAAT near the lake surface and yield the lowest elevation relative to the other two methods (Fig. 7). Therefore, our multi-proxy method resolves the contradiction of previous paleoelevation estimates, indicating a significant relief of the basin and a completely different topography during the mid-Cenozoic from today.

The low elevation of Nima basin during the late Oligocene advocated here is intriguing in that it occurred within a convergent continent-continent collision zone. Similar to this scenario, the Indus-Yarlung suture zone south of the Lhasa terrane (Fig. 1; Kapp et al., 2007) during late Oligocene-early Miocene also contained warm-water lakes that likely formed at elevations thousands of metres lower than the modern > 4.5 km elevations of Kailas Formation outcrops (DeCelles et al., 2018). Wang et al. (2015) propose a mechanism of localized thrust loading for the subsidence and low elevation of the Kailas basin in response to shortening in the south-dipping Great Counter Thrust that is on the south side next to the basin. Similarly, in the southern Nima basin the south-dipping Gaize-Siling Tso and Nima thrusts, which were established due to continued convergence between the Lhasa and Qiangtang terranes during the Cretaceous, were reactivated by the late Oligocene (DeCelles et al., 2007a). Paleocurrent and composition analyses indicate that materials of the Tertiary Nima Redbed Unit studied here are derived from southward highlands in the hanging walls of the Gaize-Siling Tso thrust and the Nima thrust (DeCelles et al., 2007a). Thereby, the mechanism of Wang et al. (2015) likely is also applicable to the Nima Basin. However, DeCelles et al. (2011, 2018) argue for the geodynamic models for the formation of low-elevation Kailas basin, in which extension and crustal thinning may take place in the upper plate of colliding orogenic system. If these geodynamic models are appropriate to the Nima Basin, the problem of lack of concurrent normal faults bounding a supposed extensional Niam Basin should be solved, which is also in suspense for the Kailas Basin (Wang et al., 2015; DeCelles et al., 2018). Regardless of specific mechanism, our findings here support that even in extreme collisions, elevation gain may be punctuated by episodes of local dynamic elevation loss (Saylor et al., 2009; DeCelles et al., 2018), hence causing a high-relief topography during the course of TP uplift and growth.

Supplementary data to this article can be found online at https://doi.org/10.1016/j.chemgeo.2018.05.041.

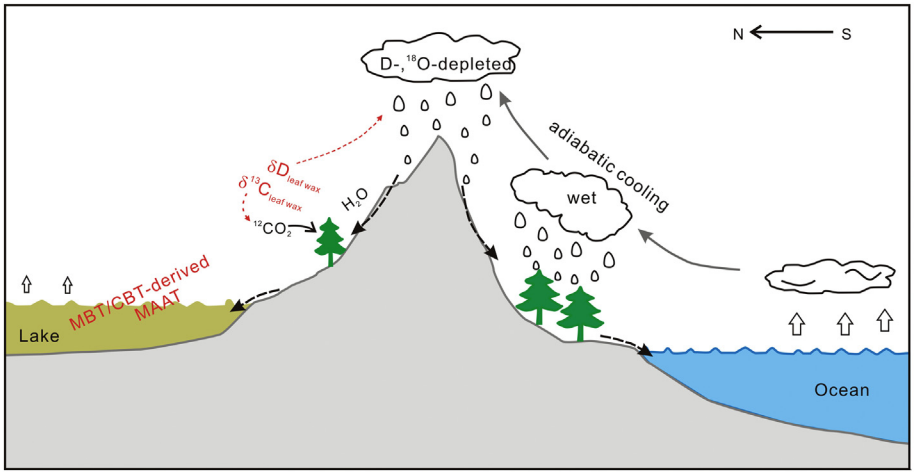

Fig. 7. A sketch showing different implications of elevation proxies in this study. Different from on the windward side, δD of leaf wax lipids on the leeward side reflects D-depleted moisture climbing over the mountain barrier that is higher than where terrestrial plants grow. Whereas $\delta^{13}C$ of leaf wax lipids reflect growth conditions determined by local elevation. BrGDGTs are mainly produced in the lake, thus reflecting near lake surface temperature. Note that this sketch is only appropriate to sites receiving moisture from a single source of the tropical Ocean as assumed in the text, and latitudinal and continental effects are neglected.

Acknowledgements

This study was supported by the "Strategic Priority Research Program" of the Chinese Academy of Sciences with grant No. XDB03020101. Yongjia Ma, Zhijie Liu and Chunsheng Jin are thanked for their efforts to collect samples. Fuli Wu kindly provided preliminary pollen data of some samples. Two anonymous reviewers are thanked for their valuable comments that help to improve this paper greatly.

References

Aichner, B., Herzschuh, U., Wilkes, H., 2010a. Influence of aquatic macrophytes on the stable carbon isotopic signatures of sedimentary organic matter in lakes on the Tibetan Plateau. Org. Geochem. 41, 706–718.
Aichner, B., Herzschuh, U., Wilkes, H., Vieth, A., Böhner, J., 2010b. δD values of n-alkanes in Tibetan lake sediments and aquatic macrophytes – a surface sediment study and application to a 16 ka record from Lake Koucha. Org. Geochem. 41, 779–790.
Araguas-Araguas, L., Froehlich, K., Rozanski, K., 2000. Deuterium and oxygen-18 isotope composition of precipitation and atmospheric moisture. Hydrol. Process. 14, 1341–1355.
Bai, Y., Fang, X., Tian, Q., 2012. Spatial patterns of soil n-alkane δD values on the Tibetan Plateau: implications for monsoon boundaries and paleoelevation reconstructions. J. Geophys. Res. 117, D20113.
Bai, Y., Fang, X., Jia, G., Sun, J., Wen, R., Ye, Y., 2015. Different altitude effect of leaf wax n-alkane δD values in surface soils along two vapor transport pathways, southeastern Tibetan Plateau. Geochim. Cosmochim. Acta 170, 94–107.
Bai, Y., Chen, C., Xu, Q., Fang, X., 2018. Paleoaltimetry potentiality of branched GDGTs from southern Tibet. Geochem. Geophys. Geosyst. 19, 551–564.
Balesdent, J., Girardin, C., Mariotti, A., 1993. Site-related ^{13}C of tree leaves and soil organic matter in a temperate forest. Ecology 74, 1713–1721.
Bird, M.I., Haberle, S.G., Chivas, A.R., 1994. Effect of altitude on the carbon-isotope composition of forest and grassland soils from Papua New Guinea. Glob. Biogeochem. Cycles 8, 13–22.
Bird, B.W., Polisar, P.J., Lei, Y., Thompson, L.G., Yao, T., Finney, B.P., Bain, D.J., Pompeani, D.P., Steinman, B.A., 2014. A Tibetan lake sediment record of Holocene Indian summer monsoon variability. Earth Planet. Sci. Lett. 399, 92–102.
Blisniuk, P.M., Stern, L.A., 2005. Stable isotope paleoaltimetry: a critical review. Am. J. Sci. 305, 1033–1074.
Brierley, C.M., Fedorov, A.V., 2010. Relative importance of meridional and zonal sea surface temperature gradients for the onset of the ice ages and Pliocene-Pleistocene climate evolution. Paleoceanography 25, PA2214.
Chen, W., Zhang, S., Ding, J., Zhang, J., Zhao, X., Zhu, L., Yang, W., Yang, T., Li, H., Wu, H., 2017. Combined paleomagnetic and geochronological study on Cretaceous strata of the Qiangtang terrane, central Tibet. Gondwana Res. 41, 373–389.
Coffinet, S., Huguet, A., Williamson, D., Fosse, C., Derenne, S., 2014. Potential of GDGTs as a temperature proxy along an altitudinal transect at Mount Rungwe (Tanzania). Org. Geochem. 68, 82–89.
Sinninghe Damsté, 2016. Spatial heterogeneity of sources of branched tetraethers in shelf systems: the geochemistry of tetraethers in the Berau River delta (Kalimantan, Indonesia). Geochim. Cosmochim. Acta 186, 13–31.
De Jonge, C., Stadnitskaia, A., Hopmans, E.C., Cherkashov, G., Fedotov, A., Sinninghe Damsté, J.S., 2014. In-situ produced branched glycerol dialkyl glycerol tetraethers in suspended particulate matter from the Yenisei River, Eastern Siberia. Geochim. Cosmochim. Acta 125, 476–491.
DeCelles, P.G., Kapp, P., Ding, L., Gehrels, G.E., 2007a. Late Cretaceous to mid-Tertiary basin evolution in the central Tibetan Plateau: changing environments in response to tectonic partitioning, aridification, and regional elevation gain. Geol. Soc. Am. Bull. 119, 654–680.
DeCelles, P.G., Quade, J., Kapp, P., Fan, M., Dettman, D., Ding, L., 2007b. High and dry in the central Tibetan Plateau during the Oligocene. Earth Planet. Sci. Lett. 253, 389–401.
DeCelles, P.G., Kapp, P., Quade, J., Gehrels, G.E., 2011. Oligocene–Miocene Kailas basin, southwestern Tibet: record of post collisional upper plate extension in the Indus-Yarlung suture zone. Geol. Soc. Am. Bull. 123, 1337–1362.
DeCelles, P.G., Castañeda, I.S., Carrapa, B., Liu, J., Quade, J., Leary, R., Zhang, L., 2018. Oligocene-Miocene great lakes in the India-Asia collision zone. Basin Res. 30, 228–247.
Deng, T., Ding, L., 2015. Paleoaltimetry reconstructions of the Tibetan Plateau: progress and contradictions. Natl. Sci. Rev. 2, 417–437.
Deng, T., Wang, S., Xie, G., Li, Q., Hou, S., Sun, B., 2012. A mammalian fossil from the Dingqing Formation in the Lunpola Basin, northern Tibet, and its relevance to age and paleo-altimetry. Chin. Sci. Bull. 57, 261–269.
Deng, L., Jia, G., Jin, C., Li, S., 2016. Warm season bias of branched GDGT temperature estimates causes underestimation of altitudinal lapse rate. Org. Geochem. 96, 11–17.
Eglinton, T.I., Eglinton, G., 2008. Molecular proxies for paleoclimatology. Earth Planet. Sci. Lett. 275, 1–16.
Ehleringer, J.R., Buchmann, N., Flanagan, L.B., 2000. Carbon isotope ratios in belowground carbon cycle processes. Ecol. Appl. 10, 412–422.
Fawcett, P.J., Werne, J.P., Anderson, R.S., Heikoop, J.M., Brown, E.T., Berke, M.A., Smith, S.J., Goff, F., Donohoo-Hurley, L., Cisneros-Dozal, L.M., Schouten, S., Sinninghe Damsté, J.S., Huang, Y.S., Toney, J., Fessenden, J., Woldegabriel, G., Atudorei, V., Geissman, J.W., Allen, C.D., 2011. Extended megadroughts in the southwestern United States during Pleistocene interglacials. Nature 470, 518–521.
Gébelin, A., Mulch, A., Teyssier, C., Jessup, M.J., Law, R.D., Brunel, M., 2013. The Miocene elevation of Mount Everest. Geology 41, 799–802.
Günther, F., Thiele, A., Gleixner, G., Xu, B., Yao, T., Schouten, S., 2014. Distribution of bacterial and archaeal ether lipids in soils and surface sediments of Tibetan lakes: implications for GDGT-based proxies in saline high mountain lakes. Org. Geochem. 67, 19–30.
Guo, X., Wang, L., Tian, L., 2015. Spatio-temporal variability of vertical gradients of major meteorological observations around the Tibetan Plateau. Int. J. Climatol. 36, 1901–1916.
Hou, J., Andrea, W.J.D., MacDonald, D., Huang, Y., 2007. Hydrogen isotopic variability in leaf waxes among terrestrial and aquatic plants around Blood Pond, Massachusetts (USA). Org. Geochem. 38, 977–984.
Hou, J., D'Andrea, W.J., Huang, Y., 2008. Can sedimentary leaf waxes record D/H ratios of continental precipitation? Field, model, and experimental assessments. Geochim. Cosmochim. Acta 72, 3503–3517.
Hren, M., Pagani, M., Erwin, D.M., Brandon, M., 2010. Biomarker reconstruction of the early Eocene paleotopography and paleoclimate of the northern Sierra Nevada. Geology 38, 7–10.
Jia, G., Chen, F.J., Peng, P.A., 2008a. Sea surface temperature differences between the western equatorial Pacific and northern South China Sea since the Pliocene and their paleoclimatic implications. Geophys. Res. Lett. 35, L18609.
Jia, G., Wei, K., Chen, F., Peng, P., 2008b. Soil n-alkane δD vs. altitude gradients along Mount Gongga, China. Geochim. Cosmochim. Acta 72, 5165–5174.
Jia, G., Li, Z., Peng, P., Zhou, L., 2012. Aeolian n-alkane isotopic evidence from North Pacific for a Late Miocene decline of C_4 plant in the arid Asian interior. Earth Planet. Sci. Lett. 321–322, 32–40.
Jia, G., Rao, Z., Zhang, J., Li, Z., Chen, F., 2013. Tetraether biomarker records from a loess-paleosol sequence in the western Chinese Loess Plateau. Front. Microbiol. 4, 199. http://dx.doi.org/10.3389/fmicb.2013.00199.
Jia, G., Bai, Y., Ma, Y., Sun, J., Peng, P., 2015. Paleoelevation of Tibetan Lunpola basin in the Oligocene–Miocene transition estimated from leaf wax lipid dual isotopes. Glob. Planet. Chang. 126, 14–22.
Kapp, P., DeCelles, P.G., Gehrels, G.E., Heizler, M., Ding, L., 2007. Geological records of the Lhasa–Qiangtang and Indo–Asian collisions in the Nima area of central Tibet. Geol. Soc. Am. Bull. 119, 917–932.
Kattel, D.B., Yao, T., Yang, K., Tian, L., Yang, G., Joswiak, D., 2013. Temperature lapse

rate in complex mountain terrain on the southern slope of the central Himalayas. Theor. Appl. Climatol. 113, 671–682.
Kelly, C.K., Woodward, F.I., 1995. Ecological correlates of carbon isotope composition of leaves: a comparative analysis testing for the effects of temperature, CO_2 and O_2 partial pressures and taxonomic relatedness on $\delta^{13}C$. J. Ecol. 83, 509–515.
Körner, C., Farquhar, G.D., Roksandic, Z., 1988. A global survey of carbon isotope discrimination in plants from high altitude. Oecologia 74, 623–632.
Körner, C., Farquhar, G.D., Wong, S.C., 1991. Carbon isotope discrimination by plants follows latitudinal and altitudinal trends. Oecologia 88, 30–40.
Li, L., Garzione, C.N., 2017. Spatial distribution and controlling factors of stable isotopes in meteoric waters on the Tibetan Plateau: implications for paleoelevation reconstruction. Earth Planet. Sci. Lett. 460, 302–314.
Li, X., Cheng, G., Lu, L., 2005. Spatial analysis of air temperature in the Qinghai-Tibet Plateau. Arct. Antarct. Alp. Res. 37, 246–252.
Li, M.C., Liu, H.Y., Yi, X.F., Li, L.X., 2006. Characterization of photosynthetic pathway of plant species growing in the eastern Tibetan plateau using stable carbon isotope composition. Photosynthetica 44, 102–108.
Li, M., Liu, H., Li, L., Yi, X., Zhu, X., 2007. Carbon isotope composition of plants along altitudinal gradient and its relationship to environmental factors on the Qinghai-Tibet Plateau. Pol. J. Ecol. 55, 67–78.
Li, J.Z., Wang, G.A., Liu, X.Z., Han, J.M., Liu, M., Liu, X.J., 2009. Variations in carbon isotope ratios of C_3 plants and distribution of C_4 plants along an altitudinal transect on the eastern slope of Mount Gongga. Sci. China Ser. D Earth Sci. 52, 1714–1723.
Liu, W.G., Huang, Y., 2005. Compound specific D/H ratios and molecular distributions of higher plant leaf waxes as novel paleoenvironmental indicators in the Chinese Loess Plateau. Org. Geochem. 36, 851–860.
Liu, H., Liu, W., 2016. n-Alkane distributions and concentrations in algae, submerged plants and terrestrial plants from the Qinghai-Tibetan Plateau. Org. Geochem. 99, 10–22.
Liu, W., Yang, H., 2008. Multiple controls for the variability of hydrogen isotopic compositions in higher plant n-alkane from modern ecosystems. Glob. Chang. Biol. 14, 2166–2177.
Liu, W., Yang, H., Li, L., 2006. Hydrogen isotopic compositions of n-alkanes from terrestrial plants correlate with their ecological life forms. Oecologia 150, 330–338.
Liu, G., Li, M., An, L., 2007. The environmental significance of stable carbon isotope composition of modern plant leaves in the northern Tibetan Plateau, China. Arct. Antarct. Alp. Res. 39, 678–681.
Liu, W., Wang, H., Zhang, C., Liu, Z., He, Y., 2013. Distribution of glycerol dialkyl glycerol tetraether lipids along an altitudinal transect on Mt. Xiangpi, NE Qinghai-Tibetan Plateau, China. Org. Geochem. 57, 76–83.
Liu, J., Liu, W., An, Z., Yang, H., 2016. Different hydrogen isotope fractionations during lipid formation in higher plants: implications for paleohydrology reconstruction at a global scale. Sci. Rep. 6, 19711.
Liu, W., Yang, H., Wang, H., Yao, Y., Wang, Z., Cao, Y., 2016. Influence of aquatic plants on the hydrogen isotope composition of sedimentary long-chain n-alkanes in the Lake Qinghai region, Qinghai-Tibet Plateau. Sci. China Earth Sci. 59, 1368–1377.
Liu-Zeng, J., Tapponnier, P., Gaudemer, Y., Ding, L., 2008. Quantifying landscape differences across the Tibetan plateau: implications for topographic relief evolution. J. Geophys. Res. 113, F04018.
Loomis, S.E., Russell, J.M., Ladd, B., Street-Perrott, F.A., Sinninghe Damsté, J.S., 2012. Calibration and application of the branched GDGT temperature proxy on East African lake sediments. Earth Planet. Sci. Lett. 357–358, 277–288.
Lü, H.Y., Wu, N., Gu, Z., Guo, Z., Wang, L., Wu, H., Wang, G., Zhou, L., Han, J., Liu, T.S., 2004. Distribution of carbon isotope composition of modern soils on the Qinghai-Tibetan Plateau. Biogeochemistry 70, 273–297.
Luo, P., Peng, P., Gleixner, G., Zheng, Z., Pang, Z., Ding, Z., 2011. Empirical relationship between leaf wax n-alkane δD and altitude in the Wuyi, Shennongjia and Tianshan Mountains, China: implications for paleoaltimetry. Earth Planet. Sci. Lett. 301, 285–296.
Männel, T.T., Auerswald, K., Schnyder, H., 2007. Altitudinal gradients of grassland carbon and nitrogen isotope composition are recorded in the hair of grazers. Glob. Ecol. Biogeogr. 16, 583–592.
Meng, J., Coe, R.S., Wang, C., Gilder, S.A., Zhao, X., Liu, H., Li, Y., Ma, P., Shi, K., Li, S., 2017. Reduced convergence within the Tibetan Plateau by 26 Ma? Geophys. Res. Lett. 44, 6624–6632.
Mokhov, I.I., Akperov, M.G., 2006. Tropospheric lapse rate and its relation to surface temperature from reanalysis data. Izv. Atmos. Oceanic Phys. 42 (4), 430–438.
Moran, T.A., Marshall, S.J., Evans, E.C., Sinclair, K.E., 2007. Altitudinal gradients of stable isotopes in lee-slope precipitation in the Canadian Rocky Mountains. Arct. Antarct. Alp. Res. 39 (3), 455–467.
Mügler, I., Sachse, D., Werner, M., Xu, B., Wu, G., Yao, T., Gleixner, G., 2008. Effect of lake evaporation on δD values of lacustrine n-alkanes: a comparison of Nam Co (Tibetan Plateau) and Holzmaar (Germany). Org. Geochem. 39, 711–729.
Mulch, A., Graham, S.A., Chamberlain, C.P., 2006. Hydrogen isotopes in Eocene river gravels and paleoelevation of the Sierra Nevada. Science 313, 87–89.
Pearson, E.J., Juggins, S., Talbot, H.M., Weckström, J., Rosén, P., Ryves, D.B., Roberts, S.J., Schmidt, R., 2011. A lacustrine GDGT-temperature calibration from the Scandinavian Arctic to Antarctic: renewed potential for the application of GDGT-paleothermometry in lakes. Geochim. Cosmochim. Acta 75, 6225–6238.
Peters, K.E., Walters, C.C., Moldowan, J.M., 2004. The Biomarker Guide, 2nd ed. Cambridge University Press, New York (451 pp.).
Peterse, F., van der Meer, M.T.J., Schouten, S., Jia, G., Ossebaar, J., Blokker, J., Sinninghe Damsté, J.S., 2009. Assessment of soil n-alkane δD and branched tetraether membrane lipid distributions as tools for paleoelevation reconstruction. Biogeosciences 6, 2799–2807.
Peterse, F., Prins, M.A., Beets, C.J., Troelstra, S.R., Zheng, H., Gu, Z., Schouten, S., Sinninghe Damsté, J.S., 2011. Decoupled warming and monsoon precipitation in East Asia over the last deglaciation. Earth Planet. Sci. Lett. 301, 256–264.
Peterse, F., van der Meer, J., Schouten, S., Weijers, J.W., Fierer, N., Jackson, R.B., Kim, J.-H., Sinninghe Damsté, J.S., 2012. Revised calibration of the MBT–CBT paleotemperature proxy based on branched tetraether membrane lipids in surface soils. Geochim. Cosmochim. Acta 96, 215–229.
Peterse, F., Vonk, J.E., Holmes, R.M., Giosan, L., Zimov, N., Eglinton, T.I., 2014. Branched glycerol dialkyl glycerol tetraethers in Arctic lake sediments: sources and implications for paleothermometry at high latitudes. J. Geophys. Res. Biogeosci. 119, 1738–1754.
Poage, M.A., Chamberlain, C.P., 2001. Empirical relationships between elevation and the stable isotope composition of precipitation and surface waters: considerations for studies of paleoelevation change. Am. J. Sci. 301, 1–15.
Poage, M.A., Chamberlain, C.P., 2002. Stable isotopic evidence for a Pre-Middle Miocene rain shadow in the western Basin and Range: implications for the paleotopography of the Sierra Nevada. Tectonics 21 (4), 1034.
Pokharel, K.P., Yohannes, E., Salvarina, I., Storch, I., 2015. Isotopic evidence for dietary niche overlap between barking deer and four-horned antelope in Nepal. J. Biol. Res. (Thessaloniki) 22, 6. http://dx.doi.org/10.1186/s40709-015-0029-0.
Polissar, P.J., Freeman, K.H., Rowley, D.B., McInerney, F.A., Currie, B.S., 2009. Paleoaltimetry of the Tibetan Plateau from D/H ratios of lipid biomarkers. Earth Planet. Sci. Lett. 287, 64–76.
Powers, J.S., Schlesinger, W.H., 2002. Geographic and vertical patterns of stable carbon isotopes in tropical rain forest soils of Costa Rica. Geoderma 109, 141–160.
Qiang, W., Wang, X., Chen, T., Feng, H., An, L., He, Y., Wang, G., 2003. Variations of stomatal density and carbon isotope values of *Picea crassifolia* at different altitudes in the Qilian Mountains. Trees 17, 258–262.
Quade, J., Breeckerm, D.O., Daëronm, M., Eilerm, J., 2011. The paleoaltimetry of Tibet: an isotopic perspective. Am. J. Sci. 311, 77–115.
Radke, J., Bechtel, A., Gaupp, R., Püttmann, W., Sachse, D., Schwark, L., Gleixner, G., 2005. Correlation between hydrogen isotope ratios of lipid biomarkers and sediment maturity. Geochim. Cosmochim. Acta 69, 5517–5530.
Ramesh, R., Sarin, M.M., 1992. Stable isotope study of the Ganga (Ganges) river system. J. Hydrol. 139, 49–62.
Rao, Z., Zhu, Z., Jia, G., Henderson, A.C.G., Xue, Qi., Wang, S., 2009. Compound specific dD values of long chain n-alkanes derived from terrestrial higher plants are indicative of the δD of meteoric waters: evidence from surface soils in eastern China. Org. Geochem. 40, 922–930.
Rowley, D.B., 2007. Stable isotope-based paleoaltimetry: theory and validation. Rev. Mineral. Geochem. 66, 23–52.
Rowley, D.B., Currie, B.C., 2006. Palaeo-altimetry of the Late Eocene to Miocene Lunpola Basin, central Tibet. Nature 439, 677–681.
Rowley, D.B., Pierrehumbert, R.T., Currie, B.S., 2001. A new approach to stable isotope-based paleoaltimetry: implications for paleoaltimetry and paleohypsometry of the High Himalaya since the Late Miocene. Earth Planet. Sci. Lett. 188, 253–268.
Sachse, D., Billault, I., Bowen, G.J., Chikaraishi, Y., Dawson, T.E., Feakins, S.J., Freeman, K.H., Magill, C.R., McInerney, F.A., van der Meer, M.T.J., Polissar, P., Robins, R.J., Sachs, J.P., Schmidt, H.-L., Sessions, A.L., White, J.W.C., West, J.B., Kahmen, A., 2012. Molecular paleohydrology: interpreting the hydrogen-isotopic composition of lipid biomarkers from photosynthesizing organisms. Annu. Rev. Earth Planet. Sci. 40, 221–249.
Saylor, J.E., Quade, J., Dettman, D., DeCelles, P.G., Kapp, P., 2009. The late Miocene through present paleoelevation history of southwestern Tibet. Am. J. Sci. 309, 1–42.
Schäfer, I.K., Lanny, V., Franke, J., Eglinton, T.I., Zech, M., Vysloužilová, B., Zech, R., 2016. Leaf waxes in litter and topsoils along a European transect. Soil 2, 551–564.
Schimmelmann, A., Sessions, A.L., Mastalerz, M., 2006. Hydrogen isotopic (D/H) composition of organic matter during diagenesis and thermal maturation. Annu. Rev. Earth Planet. Sci. 34, 501–533.
Schouten, S., Hopmans, E.C., Sinninghe Damsté, J.S., 2013. The organic geochemistry of glycerol dialkyl glycerol tetraether lipids: a review. Org. Geochem. 54, 19–61.
Shea, D.J., Trenberth, K.E., Reynolds, R.W., 1992. A global monthly sea surface temperature climatology. J. Clim. 5, 987–1001.
Sinninghe Damsté, J.S., Ossebaar, J., Schouten, S., Verschuren, D., 2008. Altitudinal shifts in the branched tetraether lipid distribution in soil from Mt. Kilimanjaro (Tanzania): implications for the MBT/CBT continental palaeothermometer. Org. Geochem. 39, 1072–1076.
Sinninghe Damsté, J.S., Ossebaar, J., Abbas, B., Schouten, S., Verschuren, D., 2009. Fluxes and distribution of tetraether lipids in an equatorial African lake: constraints on the application of the TEX_{86} palaeothermometer and BIT index in lacustrine settings. Geochim. Cosmochim. Acta 73, 4232–4249.
Sinninghe Damsté, J.S., Rijpstra, W.I.C., Hopmans, E.C., Weijers, J.W.H., Foesel, B.U., Overman, J., Dedysh, S.N., 2011. 13,16-Dimethyl octacosanedionic acid (iso-diabolic acid): a common membrane-spanning lipid of Acidobacteria subdivisions 1 and 3. Appl. Environ. Microbiol. 77, 4147–4154.
Stewart, D.R.M., Pearson, P.N., Ditchfield, P.W., Singano, J.M., 2004. Miocene tropical Indian Ocean temperatures: evidence from three exceptionally preserved foraminiferal assemblages from Tanzania. J. Afr. Earth Sci. 40, 173–190.
Stone, P.H., Carlson, J.H., 1979. Atmospheric lapse rate regimes and their parameterization. J. Atmos. Sci. 36, 415–423.
Sun, Q., Chu, G., Liu, M., Xie, M., Li, S., Ling, Y., Wang, X., Shi, L., Jia, G., Lü, H., 2011. Distributions and temperature dependence of branched glycerol dialkyl glycerol tetraethers in recent lacustrine sediments from China and Nepal. J. Geophys. Res. 116, G01008.
Sun, J.M., Xu, Q.H., Liu, W.M., Zhang, Z.Q., Xue, L., Zhao, P., 2014. Palynological evidence for the latest Oligocene–early Miocene paleoelevation estimate in the Lunpola Basin, central Tibet. Palaeogeogr. Palaeoclimatol. Palaeoecol. 399, 21–30.

Takeuchi, A., Larson, P.B., 2005. Oxygen isotope evidence for the late Cenozoic development of an orographic rain shadow in eastern Washington, USA. Geology 33, 313–316.
Tierney, J.E., Russell, J.M., 2009. Distributions of branched GDGTs in a tropical lake system: implications for lacustrine application of theMBT/CBT paleoproxy. Org. Geochem. 40, 1032–1036.
Tierney, J.E., Russell, J.M., Huang, Y.S., Sinninghe Damsté, J.S., Hopmans, E.C., Cohen, A.S., 2008. Northern Hemisphere controls on tropical southeast African climate during the past 60,000 years. Science 322, 252–255.
Tierney, J.E., Russell, J.M., Eggemont, H., Hopmans, E.C., Verschuren, D., Sinninghe Damsté, J.S., 2010a. Environmental controls on branched tetraether lipid distributions in tropical East African lake sediments: a new lacustrine paleothermometer? Geochim. Cosmochim. Acta 74, 4902–4918.
Tierney, J.E., Russell, J.M., Huang, Y., 2010b. A molecular perspective on Late Quaternary climate and vegetation change in the Lake Tanganyika basin, East Africa. Quat. Sci. Rev. 29, 787–800.
Tierney, J.E., Schouten, S., Pitcher, A., Hopmans, E.C., Sinninghe Damsté, J.S., 2012. Core and intact polar glycerol dialkyl glycerol tetraethers (GDGTs) in Sand Pond, Warwick, Rhode Island (USA): insights into the origin of lacustrine GDGTs. Geochim. Cosmochim. Acta 77, 561–581.
Tipple, B.J., Pagani, M., 2007. The early origins of terrestrial C_4 photosynthesis. Annu. Rev. Earth Planet. Sci. 35, 435–461.
Tipple, B.J., Meyers, S.R., Pagani, M., 2010. Carbon isotope ratio of Cenozoic CO_2: a comparative evaluation of available geochemical proxies. Paleoceanography 25, PA3202.
Tremblin, M., Hermoso, M., Minoletti, F., 2016. Equatorial heat accumulation as a long-term trigger of permanent Antarctic ice sheets during the Cenozoic. Proc. Natl. Acad. Sci. U. S. A. 113, 11782–11787.
Tuo, J., Zhang, M., Wang, X., Zhang, C., 2006. Hydrogen isotope ratios of aliphatic and diterpenoi hydrocarbons in coals and carbonaceous mudstones from the Liaohe Basin, China. Org. Geochem. 37, 165–176.
Van de Water, P.K., Leavitt, S.W., Betancourt, J.L., 2002. Leaf $\delta^{13}C$ variability with elevation, slope aspect, and precipitation in the Southwest United States. Oecologia 132, 332–343.
Vogts, A., Badewien, T., Rullkötter, J., Schefuß, E., 2016. Near-constant apparent hydrogen isotope fractionation between leaf wax n-alkanes and precipitation in tropical regions: evidence from a marine sediment transect off SW Africa. Org. Geochem. 96, 18–27.
Wang, N., Wu, F.X., 2015. New Oligocene cyprinid in the central Tibetan Plateau documents the pre-uplift tropical lowlands. Ichthyol. Res. 62, 274–285.
Wang, L., Lü, H., Wu, N., Wu, H., Liu, T., 2003. Altitudinal trends of stable carbon isotope composition for Poeceae in Qinghai-Xizang Plateau. Quat. Sci. 23 (5), 573–580 (In Chinese with English abstract).
Wang, Y., Kromhout, E., Zhang, C., Xu, Y., Parker, W., Deng, Tao, Qiu, Z., 2008. Stable isotopic variations in modern herbivore tooth enamel, plants and water on the Tibetan Plateau: implications for paleoclimate and paleoelevation reconstructions. Palaeogeogr. Palaeoclimatol. Palaeoecol. 260, 359–374.
Wang, Y.V., Larsen, T., Leduc, G., Andersen, N., Blanz, T., Schneider, R.R., 2013. What does leaf wax δD from amixed C_3/C_4 vegetation region tell us? Geochim. Cosmochim. Acta 111, 128–139.
Wang, E., Kamp, P.J.J., Xu, G., Hodges, K.V., Meng, K., Chen, L., Wang, G., Luo, H., 2015. Flexural bending of southern Tibet in a retro foreland setting. Sci. Rep. 5, 12076.
Wang, C., Hren, M., Hoke, G.D., Liu-Zeng, J., Garzione, C.N., 2017. Soil n-alkane δD and glycerol dialkyl glycerol tetraether (GDGT) distributions along an altitudinal transect from Southwest China: evaluating organic molecular proxies for paleoclimate and paleoelevation. Org. Geochem. 107, 21–32.
Wangda, P., Ohsawa, M., 2006. Gradational forest change along the climatically dry valley slopes of Bhutan in the midst of humid eastern Himalaya. Plant Ecol. 186, 109–128.
Wei, K., Jia, G., 2009. Soil n-alkane $\delta^{13}C$ along a mountain slope as an integrator of altitude effect on plant species $\delta^{13}C$. Geophys. Res. Lett. 36, L11401.
Weijers, J.W.H., Schefuß, E., Schouten, S., Damsté, J.S.S., 2007a. Coupled thermal and hydrological evolution of tropical Africa over the last deglaciation. Science 315, 1701–1704.
Weijers, J.W.H., Schouten, S., van den Donker, J.C., Hopmans, E.C., Sinninghe Damsté, J.S., 2007b. Environmental controls on bacterial tetraether membrane lipid distribution in soils. Geochim. Cosmochim. Acta 71, 703–713.
Wu, M.S., Feakins, S.J., Martin, R.E., Shenkin, A., Bentley, L.P., Blonder, B., Salinas, N., Asner, G.P., Malhi, Y., 2017. Altitude effect on leaf wax carbon isotopic composition in humid tropical forests. Geochim. Cosmochim. Acta 206, 1–17.
Xu, Q., Ding, L., Zhang, L., Yang, D., Cai, F., Lai, Q., Liu, J., Shi, R., 2010. Stable isotopes of modern herbivore tooth enamel in the Tibetan Plateau: implications for paleoelevation reconstructions. Chin. Sci. Bull. 55, 45–54.
Yang, Y., Ji, C., Chen, L., Ding, J., Cheng, X., Robinson, D., 2015. Edaphic rather than climatic controls over ^{13}C enrichment between soil and vegetation in alpine grasslands on the Tibetan Plateau. Funct. Ecol. 29, 839–848.
Zhang, Y.G., Pagani, M., Liu, Z., Bohaty, S.M., Deconto, R., 2013. A 40-million-year history of atmospheric CO_2. Phil. Trans. R. Soc. A 371, 20130096.
Zhao, Y., Wu, F., Fang, X., Yang, Y., 2017. Altitudinal variations in the bulk organic carbon isotopic composition of topsoil in the Qilian Mountains area, NE Tibetan Plateau, and its environmental significance. Quat. Int. 454, 45–55.